Genesis of thermalization in the three-dimensional, incompressible, Galerkin-truncated Euler equation

Sugan Durai Murugan* and Samriddhi Sankar Ray†
International Centre for Theoretical Sciences, Tata Institute of Fundamental Research, Bangalore 560089, India

(Received 6 October 2022; accepted 21 July 2023; published 28 August 2023)

The long-time solutions of the Galerkin-truncated three-dimensional, incompressible Euler equation relax to an absolute equilibrium as a consequence of phase space and kinetic-energy conservation in such a finite-dimensional system. These thermalized solutions are characterized by a Gibbs distribution of the velocity field and kinetic-energy equipartition among its (finite) Fourier modes. We now show, through detailed numerical simulations, the early stage triggers for the inevitable thermalization in physical space. Furthermore, some aspects of this process are shown to be reduced to an effective one-dimensional problem, making comparisons with the more studied Burgers equation feasible. Finally, we discuss how our understanding of the mechanism of thermalization can be exploited to numerically obtain dissipative solutions of the Euler equations and evidence for or against finite-time blowup in computer simulations.

DOI: 10.1103/PhysRevFluids.8.084605

I. INTRODUCTION

Inviscid equations of hydrodynamics which are constrained to have a finite number of Fourier modes leads to thermalized flows, which are distinctly different from our more accustomed viscous fluids. This is because Liouville's theorem ensures that the projection of the inviscid equations on a finite set of Fourier modes leads to, at long times, an inevitable thermalized, absolute equilibrium Gibbs state [1–4]. Consequently, this is accompanied by an equipartition of kinetic energy across Fourier modes $\vec{k}$ [5–7], quite unlike the celebrated Kolmogorov scaling $\sim k^{-5/3}$ associated with turbulence in three dimensions (3D) or the k^{-2} scaling of the entropy solution in the one-dimensional (1D) Burgers problem [8]. Therefore, such thermalized fluids are amenable to well-established theories of equilibrium statistical physics, whereas, being intrinsically chaotic. Recently, such nonlinear Hamiltonian systems have been used to settle questions in many-body statistical physics of ergodicity and mixing [9] as well as, admittedly in 1D, understanding vexing questions of complex-time singularities [10].

From the more specific vantage point of turbulence and fluid dynamics, the relevance of such systems is more subtle and less immediately obvious. This is particularly so for 3D turbulence where several fundamental questions remain unanswered. Hence, in the absence of the many theoretical tools available for studying the 1D Burgers equation [11], it is tempting to exploit the advantages of a 3D Galerkin-truncated incompressible Euler equation to make sense of real turbulent flows. Of course, superficially, such equilibrium solutions are in stark contrast to those obtained in (driven-dissipative) turbulence or in numerical solutions of the viscous Navier-Stokes equation. And yet the

*sugan.murugan@icts.res.in
†samriddhisankarray@gmail.com

truncated equation retains the same nonlinear triadic structure as the parent inviscid partial differential equations, or indeed, in three dimensions, the viscous Navier-Stokes equation, which models turbulent flow. Thus, in many ways, the 3D Galerkin-truncated incompressible Euler equation is a compelling link between ideas of statistical physics for a Hamiltonian system with conserved dynamics [12,13] and those which describe the behavior of out-of-equilibrium driven-dissipative viscous turbulent flows [14–16]. In the past couple of decades or so, since the work of L'vov *et al.* [17] and, subsequently, Frisch *et al.* [18], the generalization of the idea of Galerkin truncation to fine-tune triadic interactions has led to a narrowing of the gap between equilibrium statistical physics and turbulence. This, in particular, has been used most importantly in deepening our understanding of central questions in 3D turbulence such as intermittency [19–25] and the issue of bottlenecks in the energy spectrum [26–28]. Most recently, the possibilities of small-scale thermalization in real flows [29] have provided further impetus to studying the interplay of equilibrium statistical physics and turbulence, often in dimensions that are not necessarily integer [30,31].

There is another important reason why the Galerkin-truncated equation merits attention. One of the outstanding questions at the interface of physics and mathematics is the existence of weak or dissipative solutions [32–34] and the possibility of a finite-time blowup for the 3D Euler equation [35–37]. Although a review of this subject goes well beyond the scope of the present paper, suffice to say that probing the blowup problem numerically is a monumental challenge [5,38–62]. Indeed, conjectures remain speculative at best despite well-formulated criteria [63–70], which, in principle, should be easily detectable in well-resolved direct numerical simulations (DNSs) [71]. The obstacle to this, however, is that simulations are necessarily finite dimensional: The commonly used spectral simulations [72,73] solve the Galerkin-truncated and *not* the infinite-dimensional partial differential equations of inviscid flows. Hence, in finite times, which may well precede the time of blowup (as is the case for the inviscid one-dimensional Burgers equation [74,75]), the solutions thermalize (starting with the smallest scales), making methods for singularity detection, such as the analyticity strip approach [76], arduous [60,77]. Hence, for finite resolutions, in the absence of convergence of such truncated solutions (which thermalize) to the actual (weak) solutions of the Euler equations themselves, conjectures on blowups from DNSs [63,65,70,78] will remain unsettled until mechanisms to circumvent Gibbs states in mathematically self-consistent ways are discovered. The discovery of such methods is, of course, contingent on knowing how truncated equations thermalize in the first place. It is useful to recall that such methods have been discovered for the more academic 1D Burgers problem [10,79–82] owing to our thorough understanding of how the one-dimensional equation thermalizes.

Thus, the long-time chaotic Gibbs solutions [9] of the Galerkin-truncated Euler equations play contrasting roles in studies of fundamental problems in turbulence. On the one hand, they allow us to connect ideas from statistical physics to turbulence, and on the other, they remain a stumbling block in numerical methods for studying questions of blowup and dissipative solutions. This makes understanding how such 3D flows thermalize particularly essential. As a result, in recent years, since the pioneering work of Cichowlas *et al.* [6], a reasonably complete picture of how energy equipartition happens in Fourier space has emerged [6,7,83–86]. However, unlike the case of the 1D Burgers equation [74,75,79,87], not much is known of the origins of thermalization in physical space for the 3D problem.

II. THERMALIZATION

With this in mind, we perform detailed DNSs of the unit density, three-dimensional, Galerkin-truncated incompressible ($\boldsymbol{\nabla}\cdot\mathbf{u}=0$) Euler equation,

$$\frac{\partial \mathbf{u}}{\partial t} = -\mathbb{P}_{\mathrm{k_G}}[\mathbf{u}\cdot\boldsymbol{\nabla}\mathbf{u} + \boldsymbol{\nabla} p]. \tag{1}$$

The low-pass Galerkin projector $\mathbb{P}_{\mathrm{k_G}}$ sets to zero all modes of the velocity field with wave numbers larger than the prescribed Galerkin-truncation wave-number $\mathrm{k_G}$, that is $\mathbb{P}_{\mathrm{k_G}}\mathbf{u}(\mathbf{x}) = \sum_{|\mathbf{k}|\leqslant \mathrm{k_G}} e^{i\mathbf{k}\cdot\mathbf{x}}\hat{\mathbf{u}}_{\mathbf{k}}$.

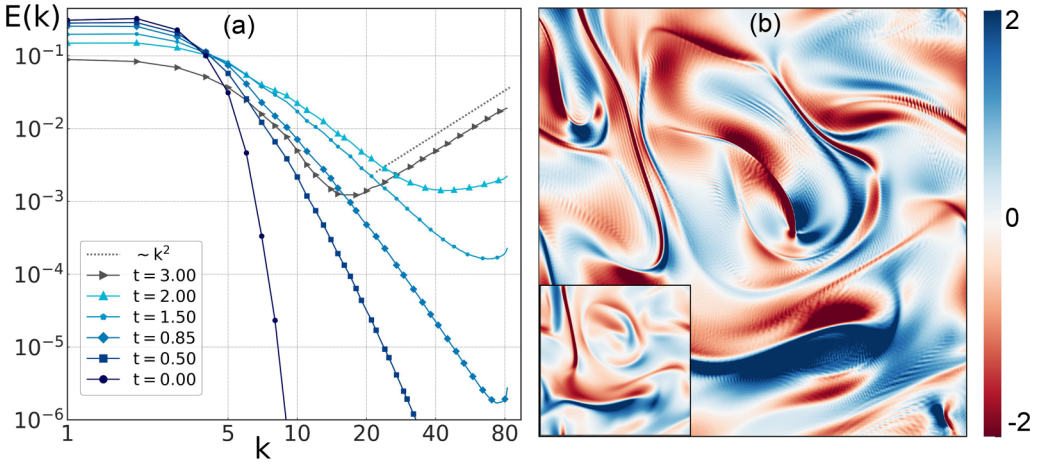

FIG. 1. (a) Log-log plots of the kinetic-energy spectrum at different times from a DNS ($N = 256$) of the Galerkin-truncated Euler equation with generic large-scale initial conditions. (b) Pseudocolor plots of the strain field component S_{yz} ($N = 512$) on the XY plane at time $t = 1.8$ where thermalization is triggered in the flow (inset at an earlier time $t = 1.2$). Although oscillatory structures are conspicuous by their absence for the former (inset), coherent streaks of oscillations with wavelengths λ_G are clearly visible for the latter. See Ref. [88] for an animation of the evolution of S_{yz} from a nonthermalized to a *fully* thermalized state.

Our DNSs use a pseudospectral method with a fourth-order Runge-Kutta scheme for time integration on 2π periodic domains with N^3 collocation points ($N = 256$ and 512) and truncation wave-number $k_G = N/3$. We have checked that our results and conclusions are consistent across simulations and choice of collocation points. We choose initial conditions (also projected on the compact Fourier domain), which has an energy spectrum of the form $E(k) \sim k^2 \exp(-k^4/k_I^4)$ to ensure that the initial energy is concentrated in the largest scales, that is, $k_I \sim O(1)$. Galerkin-truncation ensures that the kinetic energy and phase space remain conserved for all times, which, coupled with the finite dimensionality imposed by the cutoff wave-number k_G, eventually leads to a thermalized fluid with kinetic energy equipartitioned across all Fourier modes.

Given the choice of initial conditions that confines kinetic energy at large scales, the excitement of the largest wave numbers requires some time. In Fig. 1(a), we show the evolution of the kinetic-energy spectrum $E(k) \equiv \frac{1}{2} \sum_{q=k-1/2}^{k+1/2} |\hat{\mathbf{u}}(\mathbf{q})|^2$, through representative log-log plots at various instances of time. Similar evolutions of the spectrum have been reported in the first study of this kind by Cichowlas *et al.* [6].

Although a long-time thermalized fluid, through Liouville's theorem with Gibbs statistics [9] is obvious, the transition from a smooth initial condition that behaves, such as a "viscous" fluid for finite times to one that is thermalized and essentially devoid of structure is far from obvious. A clue may be found in plots of the isosurfaces of the vorticity fields as they evolve in time. In Fig. 2(a), we show a plot of the vorticity ($\boldsymbol{\omega} = \boldsymbol{\nabla} \times \mathbf{u}$) isosurface for $\sigma \leqslant |\boldsymbol{\omega}|^2 - \|\boldsymbol{\omega}\|_2^2 \leqslant 2\sigma$, where $\sigma(t)$ is the standard deviation of the enstrophy field, at early times ($t = 0.5$) when the largest available wave numbers are still not fully excited. When seen in the energy spectrum [Fig. 1(a)] at the same time, there is no sign of thermalization. These enstrophy isosurfaces are smooth and indistinguishable—as indeed the kinetic-energy spectrum at such times—from what one would expect from an extremely high Reynolds number Navier-Stokes simulations with similar initial conditions and at similar times. At slightly later times, ($t \gtrapprox 0.85$), however, isosurfaces show minute but detectable oscillatory structures [Fig. 2(b)] with wavelengths $\lambda_G = 2\pi/k_G$, reminiscent of what is seen for the corresponding problem in the one-dimensional Burgers equation [74,75,89]. We recall that a similar phenomenon was seen recently in simulations of the 3D, Galerkin-truncated *axisymmetric*

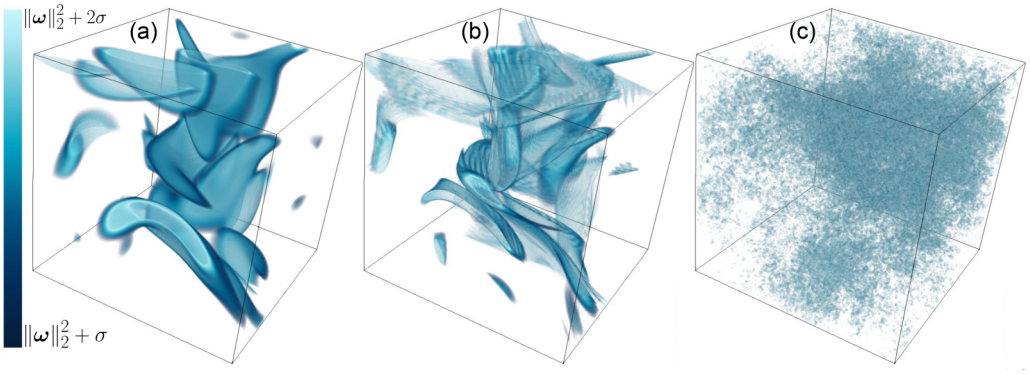

FIG. 2. Isosurfaces of the vorticity field from DNS ($N = 256$) for $\sigma \leqslant |\boldsymbol{\omega}|^2 - \|\boldsymbol{\omega}\|_2^2 \leqslant 2\sigma$ at (a) $t = 0.5$, (b) $t = 0.85$, and (c) $t = 2.5$. See Ref. [90] for an animation of the evolution of these isosurfaces from a nonthermalized to a fully thermalized state.

incompressible Euler equation [60]. These initially localized (in both physical and Fourier space) oscillations rapidly spread through the domain, with increasing amplitudes, whereas, becoming non-monochromatic. A snapshot of these fully thermalized states [Fig. 2(c)] looks noisy [82] and bears no resemblance to the well-formed isosurfaces that characterize *fully* developed turbulence or indeed solutions of the truncated equation before the onset of thermalization [Fig. 2(a)]. Consequently, the energy spectrum at such times and beyond converges to an equipartition [6] with $E(k) \sim k^2$ [Fig. 1(a)]

Although the signatures of thermalization are fairly obvious in plots such as those shown in Fig. 2, the incipient thermalized phase is best captured in visualizations of the velocity gradient. In Fig. 1(b), we show two-dimensional (XY plane) cuts of the strain field ($S_{ij} \equiv 0.5(\partial_j u_i + \partial_i u_j)$ that, at times when the effects of truncation are felt, show clear, organized oscillatory structures [panel (b)], which were absent at earlier times [*inset* in panel (a)]. We recall that in the 1D) inviscid Galerkin-truncated Burgers problem, the oscillatory structures that trigger thermalization are initially localized at point(s) comoving with the shock(s) through a resonance effect [74]. The flow we study now is fundamentally different: it is three dimensional and incompressible. So how does thermalization onsets [Figs. 2(b) and 1(b)] in the 3D Euler equations and is there an analog of resonance points or do the oscillations appear *out of the blue*?

The answer to this is delicate, and Fig. 1(b) is suggestive. Starting from initial conditions (such as the ones we have) that concentrate energy at large scales, the nonlinearity of the systems generates smaller and smaller scales in time and generates structures ranging from vortex sheets to tubes. As smaller and smaller scales get excited, many of these structures can sharpen (as thin sheets or tubes) [52,55,91] with a characteristic length scale $\sim \mathrm{k_G}^{-1}$. Such sharp structures, analogous to preshocks in the 1D Burgers equation, act as a source of *truncation waves* of wavelength λ_G—indeed the Fourier transform of the projection operator *has* a wave with wave-number $\mathrm{k_G}$—which travel along the directions in which such structures are compressed. The oscillations, of course, ensure the conservation of total kinetic energy that is a constraint in this Galerkin-truncated system. In the representative snapshot shown in Fig. 1(b), the oscillations of varying amplitudes appear not all over but in specific regions of the flow with wave vectors that, for this realization of the flow, are quite often, but not always, normal to the intense structures seen in the domain. Of course, whether such oscillations amplify or rapidly diminish in space and time is determined by the nature of the strain field locallyas we illustrate below. For oscillations that do survive, the nonlinearity allows other modes to get rapidly excited and the nonlocality of the incompressible equation allows a rapid spread of these complex oscillations across the whole domain. This eventually leads to a chaotic

thermalized fluid bereft of structure and an equipartition of kinetic energy across Fourier modes as illustrated in Fig. 2(c).

This phenomenological picture, though compelling, is difficult to *prove* in numerical simulations with the generic initial conditions that we use: The complexity of the spatial structures generated does not allow an easy way to test the different ingredients that go into the argument constructed above. In order to substantiate our theory on the genesis of oscillations in the first place, we resort to DNSs, which are controlled in a way to isolate the two different effects at play: The sharpening of velocity gradients $\nabla u \sim k_G^{-1}$ and the consequent onset of thermalization along specific directions relative to such intense structures.

III. THE ONSET OF THERMALIZATION: WHAT *MODEL FLOWS* TELL US

Among the many candidate flows—such as isolated vortex tubes and sheets—we choose to work with an initial condition consisting of two separated, opposite-signed vortex sheets (parallel to the YZ plane), located symmetrically at $x = x_1$ and $x = -x_1$, in a periodic box $[-\pi, \pi]^3$. Furthermore, these sheets have a localized perturbing flow at their centers to disturb the sheet from equilibrium. Such a flow configuration is generated by the following initial condition: For $0 \leqslant x \leqslant \pi$,

$$u_x = \mathcal{P}_\perp\left[u_0 k_\beta (x - x_1) \exp\left(-\frac{1}{2}k_\beta^2[(x-x_1)^2 + y^2 + z^2]\right)\right] \tag{2a}$$

$$u_y = \sqrt{2}\,\tanh[\gamma k_G (x - x_1)] \tag{2b}$$

$$u_z = \mathcal{P}_\perp\left[u_0 k_\beta z\, \exp\left(-\frac{1}{2}k_\beta^2[(x-x_1)^2 + y^2 + z^2]\right)\right]. \tag{2c}$$

To ensure periodicity in u_y (u_x, u_z are localized within k_β^{-1}) for $-\pi \leqslant x \leqslant 0$ the velocity field is chosen with the symmetry,

$$u_i(x, y, z) = u_i(-x, y, -z). \tag{3}$$

To ensure incompressibility, the projection operator $\mathcal{P}_\perp[\mathbf{f}] = [1 - (\nabla_\perp^{-2})\nabla_\perp(\nabla_\perp \cdot \mathbf{f})]$ on the XZ plane ($\nabla_\perp = \{\partial_x, 0, \partial_z\}$), is applied to the x and z velocities. The disturbance (u_x, u_z) here is localized at $\mathbf{x}_1 = (x_1, 0, 0)$ and $-\mathbf{x_1}$; consequently, the vortex sheet u_y is stretched for the former and compressed for the latter. The parameter γ controls the intensity of the vortex sheet and is chosen to be $1/4$ to suppress any inherent Gibbs oscillations that arise as $\gamma \to 1$. The vortex sheet locations are chosen with $x_1 = \pi/2$. We fine-tuned the extent of localization of the perturbation through k_β^{-1}, which, for the results presented here, was set to $k_\beta = 4$. Finally, the flow amplitude $u_0 = 5$ sets the energy of the perturbation field ($\sim 10^{-3}$ relative to that of the vortex sheet) as well as the timescale. This perturbing flow field with the large-scale background flow (which creates the sheet) suppressed (for clarity) is illustrated in Fig. 3(a) with the two-dimensional velocity vectors shown as green arrows superposed on the pseudocolor plot of ω_z.

By using Eqs. 2 [Fig. 3(a)] as the initial condition, we solve the Galerkin-truncated equation with $k_G = N/3$ ($N = 256$). Given the specific configuration that we chose, the center of the left sheet (at $-\mathbf{x}_1$) is compressed, whereas, the right sheet (at $\mathbf{x}_1$) is stretched [Fig. 3(b)]: As the steepening velocity gradient at $-\mathbf{x}_1$ becomes comparable to the inverse of the truncation wave number, we expect it to trigger the truncation waves in the dynamics, and the stretching at $\mathbf{x}_1$ should produce no such effect. Then, the question is: *how* and *where* do the truncation waves manifest themselves in the flow?

In the analogous 1D Burgers problem, these truncation waves emerge from the region of the preshock and are constrained to travel along the one-dimensional velocity field, and it is straightforward to identify the location of the oscillations [74]. But for the three-dimensional flows such as ours, there are infinitely many possible directions along which these oscillations, which trigger thermalization, might emerge. Indeed, if such directions are chosen randomly by the truncated

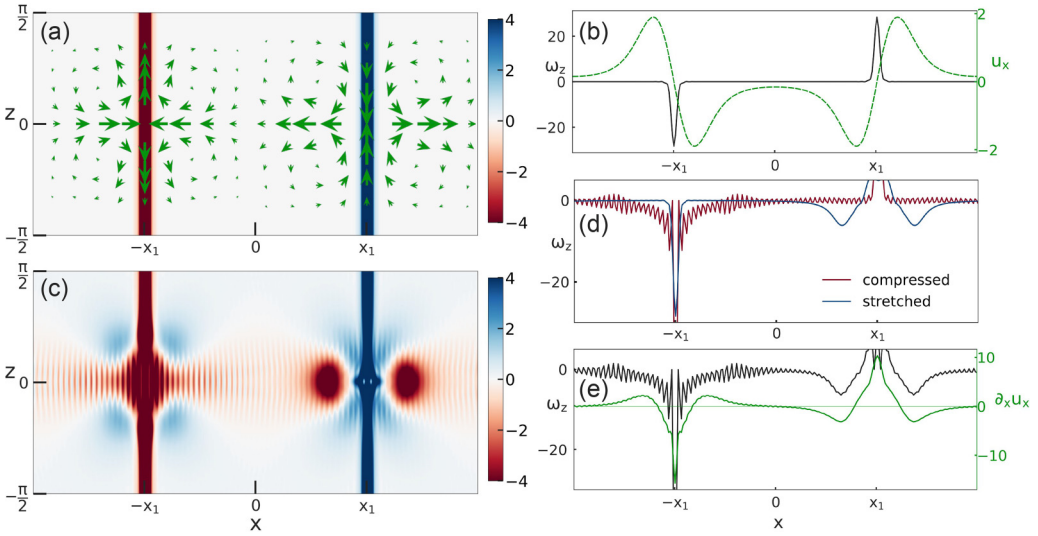

FIG. 3. Pseudocolor plots of the two-dimensional XZ plane cuts of ω_z for the model flow [Eq. (2)] at (a) $t = 0$ and (c) $t = 0.15$ with their one-dimensional (along $z = 0$) cuts (shown as black curves) in panels (b) and (e), respectively. Shown in green are the (a) instantaneous velocity vectors (u_x, u_z), (b) instantaneous velocity component u_x, and (e) the velocity gradient $\partial_x u_x$ fields. Panel (d) shows the line plot of ω_z at $t = 0.15$ when the perturbations are applied separately: Compression *(red)* at $-\mathbf{x}_1$ and stretching *(blue)* at $\mathbf{x}_1$. The initial ($t = 0$) profiles [panels (a) and (b)] are devoid of the λ_G − wavelength oscillations, which become conspicuous at later ($t = 0.15$) times as seen either (c) in the pseudocolor plots of the ω_z field or (e) in its one-dimensional cut. Naturally, these oscillations are seen just as well in (d) for the special case of compressional perturbation applied only at $-\mathbf{x}_1$. (Clearly, the stretching perturbation independently does not yield any oscillations as expected.). The absence of oscillations in panel (e) near $\mathbf{x}_1$ is subtle and discussed in the text. Reference [92] has links to an animation of the evolution of this flow to show the onset of thermalization.

dynamics, then, the problem of thermalization and, crucially, finding ways to circumvent it becomes exceptionally hard. Fortunately, as we show below, the solution to this is perhaps simpler: assuming the evidence from such model flows holds for generic initial conditions, the essential features can be mapped to an effective one-dimensional problem.

Given that these are three-dimensional flows, it is reasonable to conjecture that since the oscillations source from these sharp structures, for short times, they must be constrained to be in the same direction along which the structure is compressed. Thus, the problem of knowing where in the flow the first signs of thermalization appear may well be reduced to an effective one-dimensional problem along very specific flow lines that generate sharp structures. This conjecture is easy to check for simpler flow geometries [such as the one in Fig. 3(a) and its one-dimensional cut along $z = 0$ shown in panel (b)] where the argument leads to the inevitable conclusion that within a short time, oscillations of ω_z with wave number $\mathrm{k_G}$ appear along the $z = 0$ line (compressional direction) stemming *only* from the perturbation at $-\mathbf{x}_1$.

In Fig. 3(c), we show the solution at time $t = 0.15$. Clearly and consistent with our prediction ω_z is oscillatory with wavelength λ_G along the $z = 0$ direction. Furthermore, the perturbations at $-\mathbf{x}_1$ and $\mathbf{x}_1$ are applied independently, and the resulting line plots of ω_z along $z = 0$ line are shown in Fig. 3(d) to stress the *necessity* of a compressive eigendirection across the structure to give birth to the truncation waves.

We now return to the solution of Fig. 3(c) where both perturbations exist. By taking a one-dimensional cut along $z = 0$ in Fig. 3(c), we obtain ω_z, and the velocity gradient $S_{xx} = \partial_x u_x$, both of which are shown in Fig. 3(e). A careful reading of this figure brings to light the basic mechanism of

the onset of thermalization. The k_G − wave-number oscillations, born from the compression at $-\mathbf{x}_1$ (because of the reasons mentioned above), persist along the $z = 0$ direction and are sustained away from $-\mathbf{x}_1$ *as long as* the velocity gradient at those points is strictly non-negative. In the regions of the flow where the gradient is negative, the oscillations are suppressed. This is illustrated, for example, in Fig. 3(e) where there is a region between 0 and $\mathbf{x}_1$ with a negative gradient where the oscillations are nearly absent, in contrast with what is seen in Fig. 3(d) for the compressional case since no such negative gradients exist there. This is because the squeezing effect of the negative gradient causes the wave numbers to go beyond the truncation number k_G, resulting in their elimination through the Galerkin projector. It is important to note here that in the immediate vicinity of the source [near $-\mathbf{x}_1$ in Fig. 3(e)], the negative gradient—an integral part of the compressive structure itself—cannot suppress the oscillations. As is the case for the shock in the 1D Burgers problem, the k_G − wave-number oscillations are born continuously at $-\mathbf{x}_1$ and are, thus, always present. It is worth reminding, *en passe* , that the sharp structure at $-\mathbf{x}_1$ can also give rise to a Gibbs phenomenon—namely, the effect of summing a finite Fourier series in a region of (quasi-) discontinuity—and, hence, further oscillations. Lastly, even when the gradients become positive [in the narrow layer around $\mathbf{x}_1$ in Fig. 3(e)], the relative suppression of oscillations is due to the negative gradient on either side of this positive gradient layer, which eliminates oscillations coming from the source.

To summarize, Fig. 3 brings out the two key mechanisms responsible for the onset of thermalization in the 3D Galerkin-truncated Euler equations. First, truncation waves emerge at sharply localized structures that have, at least, one direction of compression, which squeezes them further. These play the same role as shocks do in the 1D Burgers problem [74]. Second, these oscillations, away from their place of birth, are sustained only when the flow gradient is non-negative. Crucially, the lack of a resonance effect ensures that (a) the oscillations are never spatially localized—in contrast to the 1D Burgers problem—at special points but proliferate everywhere, and (b) a relative suppression of oscillations in a positive-gradient region that lies ensconced within a negative-gradient insulating layer. A final, subtle point, also emerges from this figure. Although imposing a negative strain along their wave vector suppresses their growth [because of the truncation constraint, see Fig. 3(e)], the strain from the other eigendirections can affect them subdominantly. This can be seen in the bulge in the wave packet between $x = -x_1$ and $x = 0$ [Figs. 3(d) and 3(e)] caused by squeezing action from the u_z component.

In order to test the robustness of the claim and conclusions drawn above from Fig. 3, we rotate the disturbance field in arbitrary directions to see if the early-stage oscillations in ω_z pick out these directions every time. We choose an instance where the disturbance field u_x, u_z are rotated by $\theta = \pi/3$ from the normal of the sheet on the XZ plane for the right half of the domain $0 \leqslant x \leqslant \pi$ and symmetrically [following Eq. (3)] $\theta = \pi/6$ for the left half of the domain $-\pi \leqslant x \leqslant 0$. For this new configuration, the perturbations lead to a squeezing of the vortex sheet along the *new* compressional directions, which now are at an angle of $\pi/6$ at $-\mathbf{x}_1$ and $\pi/3$ at $\mathbf{x}_1$ away from the horizontal [indicated in Fig. 4(a) by blue and red dashed lines, respectively]. We clearly see in Fig. 4(b), consistent with our predictions, that ω_z is oscillatory in the two directions of compression for the two sheets. Thus, truncation waves are born along the compressional eigendirections as conjectured before. Although the compressional eigenvalues at both sheets are the same in magnitude by construction, evidently the amplitudes are different as seen clearly from their one-dimensional cuts along the dashed lines shown in Figs. 4(d) and 4(e). The reason is simply that the one-dimensional process sees a thicker (smoother) structure at $\mathbf{x}_1$ than at $-\mathbf{x}_1$, or in other words, the component of compressive strain across the normal direction of the sheet differs between the two cases. Although our effective one-dimensional simplified view of the thermalization onset is true *only* for arbitrarily short times and from a single source to illustrate how multiple sources interact, we present the solution at a somewhat late time ($t = 0.25$) in Fig. 4(c).

In the model flow discussed above, the parallel vortex sheets were subject to imposed perturbations. However, to make the system a bit more realistic, we now immerse the two parallel vortex sheets in a background Taylor-Green's velocity field [6], given by $u_x^{TG} = \cos x \sin y \cos z$,

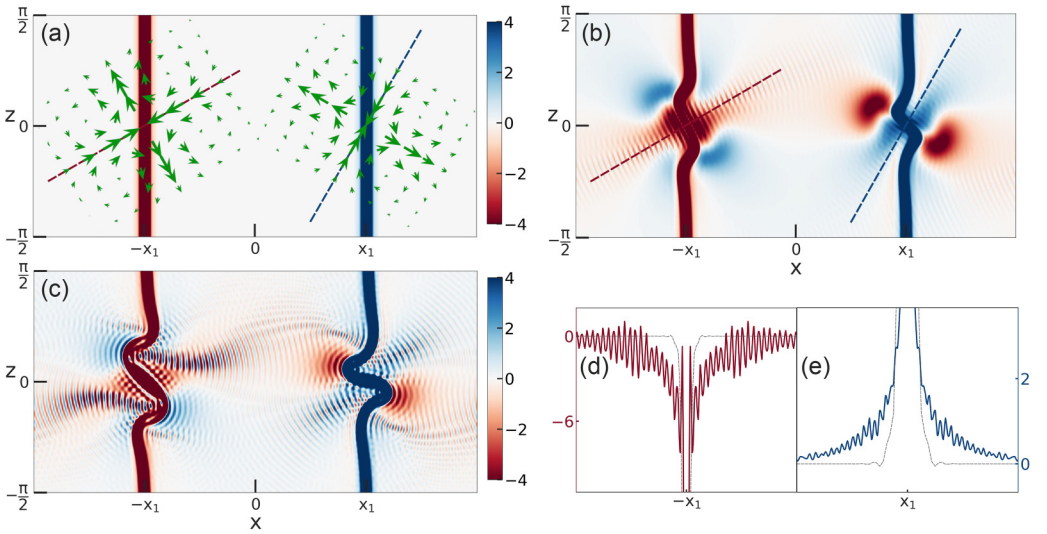

FIG. 4. Pseudocolor plots of two-dimensional XZ plane cuts of ω_z for the *rotated* model flow at (a) $t = 0$ [superimposed with the velocity vectors (u_x, u_z)], (b) $t = 0.12$, and (c) $t = 0.25$. Along the compressional directions [dashed red and blue lines in panels (a) and (b)], clear oscillations of ω_z are seen at times $t > 0$. This is shown in panel (b) as well as illustrated further by their one-dimensional cuts, shown in panels (d) and (e). In panel (c), which is at at later time, the surfacing of multiple truncation wave sources and lead to a proliferated spread of oscillations in the domain. See Ref. [93] for an animation of the evolution of this flow to show the onset of thermalization.

$u_y^{\mathrm{TG}} = -\sin x \cos y \cos z$ and evolve this system in time by using the Galerkin-truncated Euler equation. Thus, the initial condition [Fig. 5(a)] for a periodic domain of $(x, y, z) \epsilon [-2\pi, 2\pi] \times [-\pi, \pi] \times [-\pi, \pi]$, is of the form

$$u_x = \varepsilon u_x^{\mathrm{TG}}, \tag{4a}$$

$$u_y = \varepsilon u_y^{\mathrm{TG}} + A u_y^{\mathrm{SH}}, \quad u_y^{\mathrm{SH}} = 1 + \tanh[\gamma \mathrm{k_G}(\mathrm{sgn}(x)x - x_1)], \quad x_1 = \pi, \tag{4b}$$

$$u_z = 0, \tag{4c}$$

and the parameters are chosen to be $\gamma = 0.4$, $x_1 = 3\pi/2$. The ratio of energy between Taylor-Green's flow and vortex sheet is taken to be 0.1. With total energy set to unity, this fixes ε and A in Eq. (4).

Unlike the imposed localized perturbations before (see Fig. 3) that compresses the sheet directly in this case the evolution of a large-scale background Taylor-Green's flow causes the sheets to *bend* initially, leading to thinning and compression. This can be seen from the initial condition [Eq. (4)], where $S_{xx} = 0$ along both sheets ($x = \pm x_1$) and for $t \geqslant 0$ the component u_x starts to bend the sheet, followed by the shear from the component u_y^{SH}. Hence, this compression leads to the development of sharper gradients and the eventual trigger of λ_{G} − wavelength oscillations in the vorticity field ω_z. In Fig. 5(b), we show a representative snapshot of the ω_z field at $t = 0.8$ where the bent sheets get compressed and stretched in different regions. These compressed regions become sources of truncation waves and produce streaks of oscillations in the ω_z field.

The use of the background Taylor-Green's flow validates our earlier predictions and conclusions in a more general flow configuration. Figure 5(c) shows the strain field S_{xx} at $t = 0.8$, and we observe that there is a clear correlation between regions with $S_{xx} \geqslant 0$ (in *blue*) and regions with oscillations of ω_z [see Fig. 5(b)]. [A caveat: Although the oscillations in Fig. 5(b) seem to be not oriented horizontally, our choice of the strain field S_{xx} for comparison is motivated by the fact that

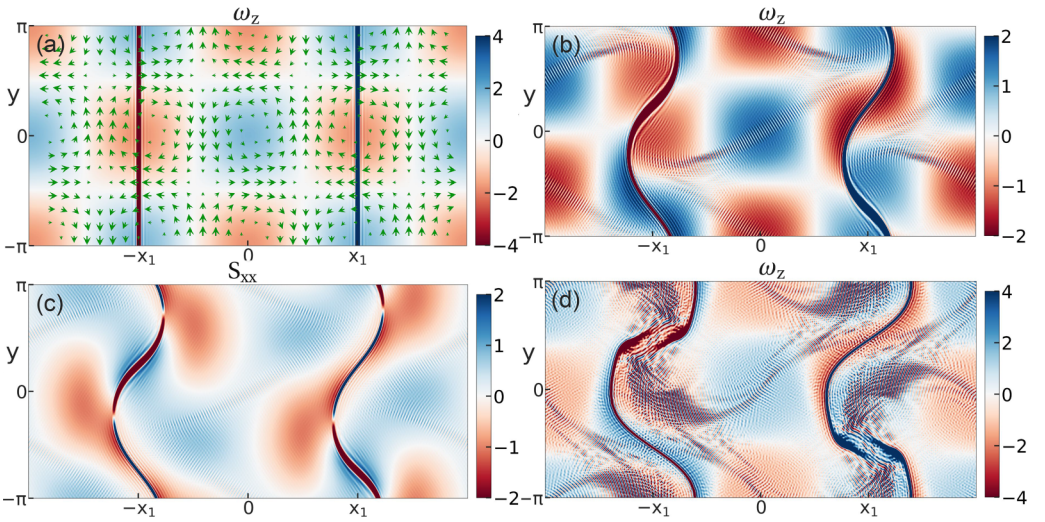

FIG. 5. Pseudocolor plots of the two-dimensional XY cut of ω_z for a pair of vortex sheets advected by a Taylor-Green's flow [Eq. (4)] at (a) $t = 0$ [along with the velocity vectors (u_x, u_z)], (b) $t = 0.8$, and (d) $t = 1.5$. show a proliferation of oscillations in time. Shown in panel (c) is the strain component S_{xx} (at $t = 0.8$). A correlation can be seen between positive strain $S_{xx} > 0$ (*blue*) and the sustained oscillations in ω_z by comparing panels (b) and (c). The link in Ref. [94] shows the full evolution of this flow up to the onset of thermalization.

initially almost all of the oscillations were along the x axis. Furthermore, the fact that the strain and vorticity fields are coupled through the evolution equations leads to faint oscillations in S_{xx} as well.) Finally, as seen in Fig. 5(d), this correlation persists even for a later time ($t = 1.5$) when there is further amplification of thermalization hot spots.

As a final example featuring a different geometrical vortical structure, we simulate a vortex filament (Fig. 6) under the Galerkin-truncated Euler equation to illustrate the nature of the onset of thermalization in a one-dimensional intense structure. The initial condition we chose to study is a stationary vortex filament together with a locally radially compressing flow: in cylindrical coordinates,

$$u_\theta(r) = \gamma \mathrm{k_G} r \, \exp\left(-\frac{1}{2}(\gamma \mathrm{k_G} r)^2\right), \tag{5a}$$

$$u_r(r, z, \theta) = -u_0 \mathrm{k}_\beta r\left(\frac{1}{2} - \frac{1}{2}(\mathrm{k}_\beta z)^2\right) \exp\left(-\frac{\mathrm{k}_\beta^2}{2}[r^2 + z^2]\right) \cos^2\theta, \tag{5b}$$

$$u_z(r, z, \theta) = u_0 \mathrm{k}_\beta z\left(1 - \frac{1}{2}(\mathrm{k}_\beta r)^2\right) \exp\left(-\frac{\mathrm{k}_\beta^2}{2}[r^2 + z^2]\right) \cos^2\theta. \tag{5c}$$

Once again, this cylindrical vortex (u_θ), whose thickness is determined by $\gamma = 0.25$, is immersed in a large-scale background flow (u_r, u_z), that perturbs the filament within a range of $\mathrm{k}_\beta^{-1} = \pi/4$ and with an amplitude of $u_0 = 10$. Note that the presence of $\cos^2\theta$ in Eq. (5) induces a generic three-dimensional perturbation in an otherwise axi-symmetric flow. Hence, the radial velocity u_r compresses the filament near $z = 0$, most along the $\theta = 0$ direction (x axis), gradually losing strength all the way to zero for $\theta = \pi/2$ as depicted in Fig. 6(a). Not surprising, the evolution of this initial condition [Eq. (5)] with the truncated Euler equations leads to oscillations that are radial with the filament at its core [Fig. 6(c)]. The difference in the compressive eigenvalue along different radial lines [shown by red, orange, and blue lines in Fig. 6(a)] reflects in the corresponding strength

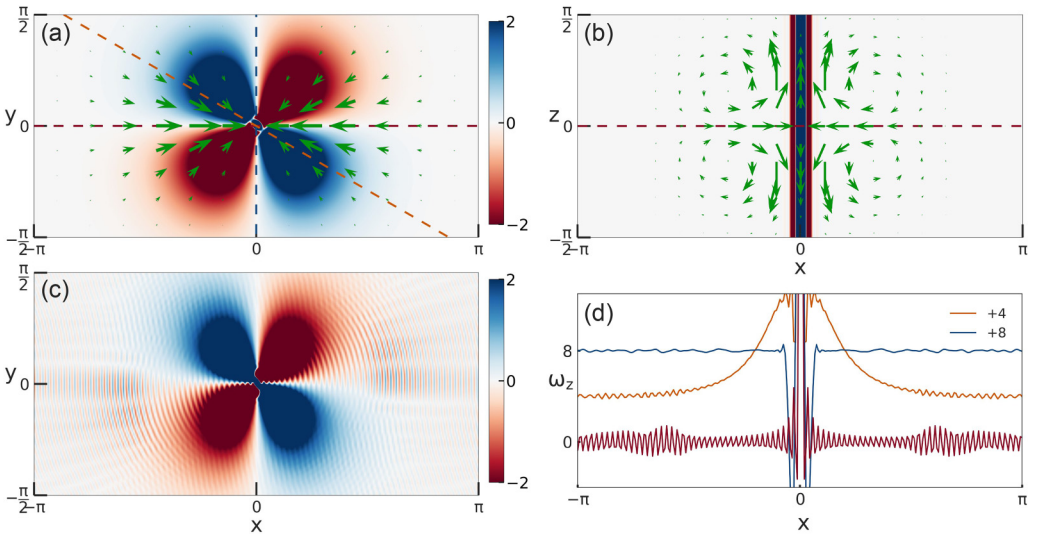

FIG. 6. Pseudocolor plots of ω_z at $t = 0$ across (a) XY (b) XZ planes; the green arrows indicate the velocity components u_r and u_z, respectively. Panel (c) shows ω_z at a later time $t = 0.12$ with radially spreading oscillations. In panel (d), the asymmetry in the strength of the oscillations at different angles is illustrated in the line plots of ω_z across $\theta = 0$ (red), $\theta = \pi/6$ (orange), and $\theta = \pi/2$ (blue); these directions were already indicated as dashed lines with the same color in panel (a). See Ref. [95] for an animation of the evolution of this flow to show the onset of thermalization.

of oscillations seen in the line plot of the vorticity ω_z along those lines in Fig. 6(d). Furthermore, the oscillations are amplified for $r \gtrsim \pi/2$ because of the support from the background flow.

IV. THE PHENOMENOLOGICAL PICTURE

In all the model flows studied above, consistent with our hypothesis, the intense structures become a source of truncation waves and sustain oscillations along the compressional eigendirection. It is crucial that we emphasize two important points in our findings: (1) The compressional eigendirection of the strain field near the extreme structures need not be perpendicular to the structures themselves, but the strength of the oscillations appearing is proportional to the component of compressive strain along the normal [depicted in Figs. 4(d) and 4(e)]. (2) The oscillations born along the compressional eigendirection grow in amplitude when the strain along the direction is positive. Thus, whereas, the fluid has to be compressive (locally) only near the structure, along that compressive eigendirection, far from the structure, the positive strain is *essential* to support and sustain the growth of the oscillations and, hence, eventual thermalization. Indeed, a negative strain here would lead to the damping of oscillations and the suppression of the onset of thermalization. The corresponding problem for the 1D Burgers equation is actually a special case of this phenomenon: In one-dimensional space, the flow is compressional, and, hence, the oscillations, trivially seen in the velocity profile, accumulate at resonance points, leading to (at early times) spatially localized structures christened *tygers* [74].

Therefore, we have now demonstrated, through numerical experiments with such specialized initial conditions, that the onset of thermalization in a *generic* three-dimensional truncated system can be seen as a superposition of processes that are essentially one dimensional: At very short times, monochromatic oscillations arise along the compressional directions associated with fluid structures with critical velocity gradients in regions supported by fluid strain. Although this was implicit for generic large-scale initial conditions, which are used to solve the Galerkin-truncated Euler equation,

the use of such special flows is essential to making this phenomenon evident. In more generic flows, such extreme velocity-gradient structures proliferate the flow and emerge at different times. Hence, each of these structures can act as a sources of truncation waves. Although, as our extensive analysis of model flows suggests, these are born individually from each *source*, before long they superpose, amplify, generate other harmonics, and eventually lead to thermalization.

To summarize, the onset of thermalization requires the conspiracy of two key ingredients. First, sufficiently sharp fluid structures that are compressed lead to truncation waves and, hence, oscillations of wavelength λ_G. This is perfectly analogous to the role shocks play in the well-understood problem of the 1D Burgers equation [74,75]. Second, in the vicinity of these structures, the flow must have a non-negative strain to sustain such oscillations. This is essential because a negative strain would lead to squeezing and the generation of harmonics with wave numbers in excess of k_G: Such higher harmonics would get expunged because of the truncation constraint that allows only modes with wave numbers $\leqslant k_G$. Although there are essential points of similarity between the analogous 1D Burgers problem, there are also crucial differences. Apart from the complexity of this phenomenon in three dimensions relative to the 1D problem—and, hence, the need to resort to model flows—what makes the present problem unique is the lack of resonance points where oscillations can accumulate and grow.

V. SUPPRESSING THERMALIZATION: DISSIPATIVE SOLUTIONS

This observation of the precise mechanism at the heart of thermalization in 3D flows is particularly important to devise numerical strategies to arrest thermalization for the reasons discussed before. Understanding how finite-dimensional equations of hydrodynamics thermalize is one aspect of this paper—but perhaps the more important question relates to whether this understanding can be exploited to devise more efficient algorithms for numerical constructions of dissipative solutions of the Euler equations and indeed conjectures for finite-time blowup through methods, such as the analyticity strip [60,76,77].

Operationally, this would involve suppressing the oscillations that trigger the flow to thermalize—making analyticity strip approaches to singularity detection [77] impractical—and ensuring conservation of energy and, thus, the lack of dissipative solutions. From our DNSs, it seems that a useful starting point would be a suitable filtering of the velocity gradient field to remove the oscillatory structures.

We suggest an algorithm to be applied to the vorticity field $\boldsymbol{\omega}$, that reconstructs a new vorticity field $\boldsymbol{\omega}^*$ in a self-consistent way that preserves the small-scale intense structures whereas, discarding the oscillations. We adapt the method developed by Hamlington *et al.* [96] to decompose the strain field into local and nonlocal (background) contributions. This is trivially performed for the vorticity field in Fourier space via

$$\hat{\omega}^{(\mathrm{NL})}(\mathbf{k}) = f(kR)\hat{\omega}(\mathbf{k}), \tag{6}$$

$$\hat{\omega}^{(L)}(\mathbf{k}) = \hat{\omega}(\mathbf{k}) - \hat{\omega}^{(\mathrm{NL})}(\mathbf{k}), \tag{7}$$

where the *hat* denotes the Fourier space ($k = |\mathbf{k}|$), the subscripts L and NL stand for the local and nonlocal contributions, respectively, and the filter,

$$f(kR) = \frac{3[\sin(kR) - kR\,\cos(kR)]}{(kR)^3} \tag{8}$$

is the Fourier transform of the three-dimensional complementary Heaviside function in spherical coordinates. Such a filter, by definition, ensures that the function on which it acts—namely, the vorticity field in this case—is *smoothed* by averaging out over a sphere of radius $R = \lambda_G$. Evidently, the local contribution $\boldsymbol{\omega}^L$ alone contains all the oscillations, and, hence, the "reconstructed" field $\boldsymbol{\omega}^* \equiv \boldsymbol{\omega}^{\mathrm{NL}}$ with $\boldsymbol{\omega}^L$ suppressed should be free of oscillations. Hence, such a *dynamic* filtering

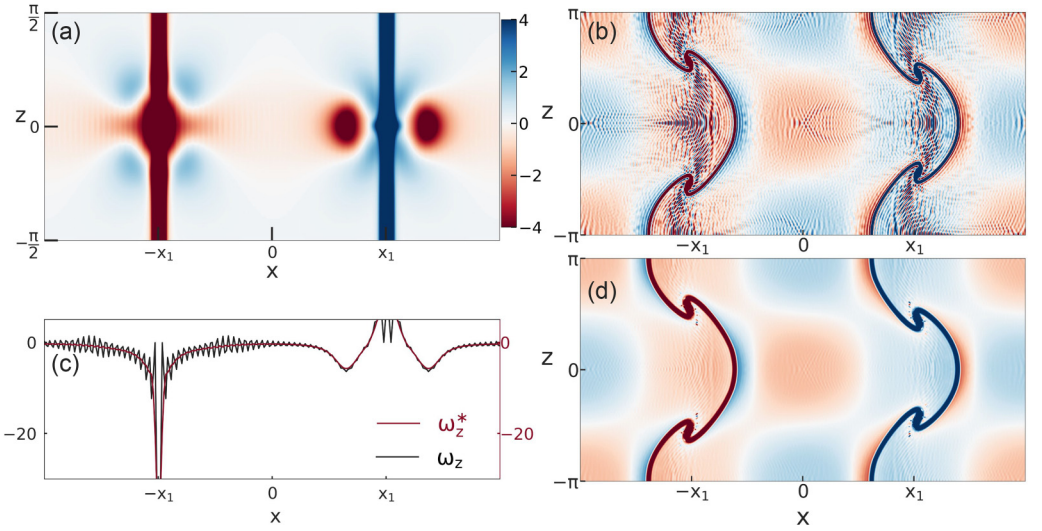

FIG. 7. (a) Pseudocolor plot of the two-dimensional XZ plane cut of the reconstructed vorticity field ω_z^* for the model flow [Eq. (2)] at $t = 0.15$. A comparison with the corresponding figure [Fig. 3(c)] for the truncated simulation shows a significant suppression of the oscillations. This is quantified in panel (c) through one-dimensional cuts (along $z = 0$) of ω_z [same as in Fig. 3(e)] and ω_z^* as a function of x. Panel (b) shows ω_z at $t = 1.5$ extracted from the Taylor-Green's flow [Eq. (4)] along the XZ plane. This is contrasted with panel (d) showing the reconstructed vorticity field ω_z^* from it, which retains the intense structures, whereas, significantly suppressing the oscillations, which would lead to thermalized solutions.

technique, namely, solving the truncated 3D Euler by recovering $\boldsymbol{\omega}^*$ and using this field to evolve at every time step, should yield a nonthermalizing, dissipative flow.

However, such an approach has the disadvantage, that along with the oscillations, the small-scale intense vortical structures are lost as well. We, therefore, adapt this idea of decomposing the field in a way that preserves the small-scale structures as far as possible and yet suppresses the oscillatory triggers of thermalization. Thus, we propose a reconstructed field as

$$\boldsymbol{\omega}^*(\mathbf{x}) = \boldsymbol{\omega}^{(\mathrm{NL})}(\mathbf{x}) + \Gamma_{2m}(\mathbf{x})\boldsymbol{\omega}^{(L)}(\mathbf{x}), \tag{9}$$

$$\Gamma_{2m}(\mathbf{x}) := \mathrm{erf}\left[\frac{|\boldsymbol{\omega}|^{2m}}{\|\boldsymbol{\omega}\|_{2m}^{2m}}\right], \tag{10}$$

where the additional regularization parameter Γ_{2m} allows us to capture the essential, intense local vortical regions, whereas, still filtering out the oscillations in the flow. The L_{2m} norm used in the definition of Γ_{2m} controls threshold level of that vortical regions we want to retain in the reconstructed field.

Although this method needs to be refined and rigorously examined in future studies for generic flow fields, we provide results from preliminary tests conducted on the model flow defined by Eq. (2). In Fig. 7(a), we show the reconstructed vorticity field at $t = 0.15$ for $m = 4$, corresponding to the plot shown in Fig. 3(c). Similarly, in Figs. 7(b) and 7(d), the vorticity field ω_z (along the XZ plane) from the solution to the Taylor-Green's initial condition [Eq. (4)] and its repaired field ω_z^* are shown.

A visual comparison of the two vorticity fields shows that our reconstruction strategy indeed leads to a significant reduction in the oscillations, whereas, still preserving the intense structures, namely, the vortical sheets in this case. This is quantified in Fig. 7(c) by comparing the z component of the vorticity along the x axis ($z = 0$) in the middle of the domain for the truncated (ω_z) and

reconstructed fields (ω_z^*). We clearly see that the oscillations responsible for thermalization, seen in ω_z, more or less vanish on reconstruction as seen in the plot. Furthermore, our use of the regularization parameter Γ_{2m} does fully preserve the intense structure in the form of vortex sheets as seen by the near overlap of ω_z and ω_z^* at $-\mathbf{x}_1$ and $\mathbf{x}_1$.

Although Fig. 7(c) seems to underline the success of this strategy—at least, for such a curated flow—the illustrative flow field shown in panels (a) and (d) still retains some traces of the oscillations. There are, at least, two reasons why this is so: (1) In our tests, we have not filtered and reconstructed the field at every time step, but, only as a proof of principle now, used this as a *static* filter and reconstruction at $t = 0.15$ [for panel (a)] and at $t = 1.5$ [for panel (d)]. A dynamic filter as discussed above, is essential, and perhaps the frequency—the time intervals between successive filtering—with which the filter should be applied needs further investigation. The latter may well be a delicate point as shown in Ref. [81] for Fourier space purging in the 1D Burgers equation. (2) Our preliminary explorations with different sharpnesses of the regularization parameter Γ_{2m} show that this, not surprisingly, is critically important for more effective suppression of thermalization hot spots, especially in the vicinity of flow structures with intense gradients. This will become crucial when such strategies are investigated systematically in a generic 3D flows.

Our preliminary results, albeit based on such a *static* filter for the model flow, show encouraging signs that such approaches may well diminish the precursor to small-scale thermalization and allow (a) dissipative solutions and (b) extending the analyticity strip method for singularity detection to longer times than currently possible. This approach, thus, complements other ongoing efforts such as that by Fehn *et al.* [97], who use a discontinuous Galerkin discretization to obtain dissipative solutions from simulations of the finite-dimensional Euler equation.

ACKNOWLEDGMENTS

We acknowledge insightful remarks by M. E. Brachet and R. Kerr and important suggestions on the paper by N. Fehn, S. S. V. Kolluru, and R. Pandit. S.S.R. is also indebted to U. Frisch for several discussions on this subject over many years. The simulations were performed on the ICTS clusters *Tetris* and *Contra*. S.S.R. acknowledges SERB-DST (India) Projects No. MTR/2019/001553, No. STR/2021/000023, and No. CRG/2021/002766 for financial support. S.S.R. would like to thank the Isaac Newton Institute for Mathematical Sciences for their support and hospitality during the program *Mathematical aspects of turbulence: where do we stand?* (EPSRC Grant No. EP/R014604/1) when part of this work was performed. We acknowledge the support of the DAEGovt. of India under Projects No. 12-R&D-TFR-5.10-1100 and No. RTI4001.

[1] E. Hopf, Statistical hydromechanics and functional calculus, J. Ration. Mech. Anal. **1**, 87 (1952).
[2] T. D. Lee and C. N. Yang, Statistical Theory of equations of state and phase transitions. II. lattice gas and ising model, Phys. Rev. **87**, 410 (1952).
[3] R. H. Kraichnan, Inertial ranges in two-dimensional turbulence, Phys. Fluids **10**, 1417 (1967).
[4] R. H. Kraichnan, Helical turbulence and absolute equilibrium, J. Fluid Mech. **59**, 745 (1973).
[5] C. Cichowlas and M. E. Brachet, Evolution of complex singularities in kida–pelz and taylor–green inviscid flows, Fluid Dyn. Res. **36**, 239 (2005).
[6] C. Cichowlas, P. Bonaïti, F. Debbasch, and M. Brachet, Effective Dissipation and Turbulence in Spectrally Truncated Euler Flows, Phys. Rev. Lett. **95**, 264502 (2005).
[7] G. Krstulovic and M. E. Brachet, Two-fluid model of the truncated Euler equations, Physica D **237**, 2015 (2008).
[8] E. Hopf, The partial differential equation $u_t + uu_x = \mu_{xx}$, Commun. Pure Appl. Math. **3**, 201 (1950).
[9] S. D. Murugan, D. Kumar, S. Bhattacharjee, and S. S. Ray, Many-Body Chaos in Thermalized Fluids, Phys. Rev. Lett. **127**, 124501 (2021).

[10] C. Rampf, U. Frisch, and O. Hahn, Eye of the tyger: Early-time resonances and singularities in the inviscid Burgers equation, Phys. Rev. Fluids **7**, 104610 (2022).
[11] J. Bec and K. Khanin, Burgers turbulence, Phys. Rep. **447**, 1 (2007).
[12] H. A. Rose, and P. L. Sulem, Fully developed turbulence and statistical mechanics, J. Phys. France **39**, 441 (1978).
[13] S. A. Orszag, Analytical theories of turbulence, J. Fluid Mech. **41**, 363 (1970).
[14] U. Frisch, *Turbulence: The Legacy of A. N. Kolmogorov* (Cambridge University Press, Cambridge, UK, 1995).
[15] R. H. Kraichnan, The structure of isotropic turbulence at very high Reynolds numbers, J. Fluid Mech. **5**, 497 (1959).
[16] A. N. Kolmogorov, V. Levin, J. C. R. Hunt, O. M. Phillips, and D. Williams, The local structure of turbulence in incompressible viscous fluid for very large Reynolds numbers, Proc. R. Soc. London, Ser. A **434**, 9 (1991).
[17] V. S. L'vov, A. Pomyalov, and I. Procaccia, Quasi-Gaussian Statistics of Hydrodynamic Turbulence in $\frac{4}{3}+\epsilon$ Dimensions, Phys. Rev. Lett. **89**, 064501 (2002).
[18] U. Frisch, A. Pomyalov, I. Procaccia, and S. S. Ray, Turbulence in Noninteger Dimensions by Fractal Fourier Decimation, Phys. Rev. Lett. **108**, 074501 (2012).
[19] A. S. Lanotte, R. Benzi, S. K. Malapaka, F. Toschi, and L. Biferale, Turbulence on a Fractal Fourier Set, Phys. Rev. Lett. **115**, 264502 (2015).
[20] A. S. Lanotte, S. K. Malapaka, and L. Biferale, On the vortex dynamics in fractal Fourier turbulence, Eur. Phys. J. E **39**, 49 (2016).
[21] M. Buzzicotti, L. Biferale, U. Frisch, and S. S. Ray, Intermittency in fractal Fourier hydrodynamics: Lessons from the Burgers equation, Phys. Rev. E **93**, 033109 (2016).
[22] M. Buzzicotti, A. Bhatnagar, L. Biferale, A. S. Lanotte, and S. S. Ray, Lagrangian statistics for Navier-Stokes turbulence under Fourier-mode reduction: fractal and homogeneous decimations, New J. Phys. **18**, 113047 (2016).
[23] S. S. Ray, Non-intermittent turbulence: Lagrangian chaos and irreversibility, Phys. Rev. Fluids **3**, 072601(R) (2018).
[24] R. Tom and S. S. Ray, Revisiting the SABRA model: Statics and dynamics, Europhys. Lett. **120**, 34002 (2017).
[25] J. R. Picardo, A. Bhatnagar, and S. S. Ray, Lagrangian irreversibility and Eulerian dissipation in fully developed turbulence, Phys. Rev. Fluids **5**, 042601(R) (2020).
[26] U. Frisch, S. Kurien, R. Pandit, W. Pauls, S. S. Ray, A. Wirth, and J.-Z. Zhu, Hyperviscosity, Galerkin Truncation, and Bottlenecks in Turbulence, Phys. Rev. Lett. **101**, 144501 (2008).
[27] U. Frisch, S. S. Ray, G. Sahoo, D. Banerjee, and R. Pandit, Real-Space Manifestations of Bottlenecks in Turbulence Spectra, Phys. Rev. Lett. **110**, 064501 (2013).
[28] D. Banerjee and S. S. Ray, Transition from dissipative to conservative dynamics in equations of hydrodynamics, Phys. Rev. E **90**, 041001(R) (2014).
[29] D. Bandak, N. Goldenfeld, A. A. Mailybaev, and G. Eyink, Dissipation-range fluid turbulence and thermal noise, Phys. Rev. E **105**, 065113 (2022).
[30] J. D. Fournier and U. Frisch, d-dimensional turbulence, Phys. Rev. A **17**, 747 (1978).
[31] A. Celani, S. Musacchio, and D. Vincenzi, Turbulence in More than Two and Less than Three Dimensions, Phys. Rev. Lett. **104**, 184506 (2010).
[32] J. Leray and R. Terrell, On the motion of a viscous liquid filling space, arXiv:1604.02484.
[33] L. Onsager, Statistical hydrodynamics, Nuovo Cimento **6**, 279 (1949).
[34] T. Buckmaster, C. De Lellis, L. Székelyhidi Jr., and V. Vicol, Onsager's Conjecture for Admissible Weak Solutions, Commun. Pure Appl. Math. **72**, 229 (2019).
[35] J. D. Gibbon, The three-dimensional Euler equations: Where do we stand? Physica D **237**, 1894 (2008).
[36] J. D. Gibbon, M. D. Bustamante, and R. M. Kerr, The three-dimensional Euler equations: singular or non-singular? Nonlinearity **21**, T123 (2008).
[37] U. Frisch, T. Matsumoto, and J. Bec, Singularities of Euler Flow? Not Out of the Blue! J. Stat. Phys. **113**, 761 (2003).

[38] M. E. Brachet, D. I. Meiron, S. A. Orszag, B. G. Nickel, R. H. Morf, and U. Frisch, Small-scale structure of the Taylor–Green vortex, J. Fluid Mech. **130**, 411 (1983).
[39] M. E. Brachet, M. Meneguzzi, A. Vincent, H. Politano, and P. L. Sulem, Numerical evidence of smooth self-similar dynamics and possibility of subsequent collapse for three-dimensional ideal flows, Phys. Fluids A **4**, 2845 (1992).
[40] O. N. Boratav, R. B. Pelz, and N. J. Zabusky, Reconnection in orthogonally interacting vortex tubes: Direct numerical simulations and quantifications, Phys. Fluids A **4**, 581 (1992).
[41] R. M. Kerr, Evidence for a singularity of the three-dimensional, incompressible Euler equations, Phys. Fluids A **5**, 1725 (1993).
[42] M. J. Shelley, D. I. Meiron, and S. A. Orszag, Dynamical aspects of vortex reconnection of perturbed anti-parallel vortex tubes, J. Fluid Mech. **246**, 613 (1993).
[43] O. N. Boratav and R. B. Pelz, Direct numerical simulation of transition to turbulence from a high-symmetry initial condition, Phys. Fluids **6**, 2757 (1994).
[44] R. M. Kerr, Velocity and scaling of collapsing Euler vortices, Phys. Fluids **17**, 075103 (2005).
[45] R. B. Pelz and K. Ohkitani, Linearly strained flows with and without boundaries - The regularizing effect of the pressure term, Fluid Dyn. Res. **36**, 193 (2005).
[46] T. Y. Hou and R. Li, Dynamic Depletion of Vortex Stretching and Non-Blowup of the 3-D Incompressible Euler Equations, J. Nonlinear Sci. **16**, 639 (2006).
[47] G. Luo and T. Y. Hou, Potentially singular solutions of the 3D axisymmetric Euler equations, Proc. Natl. Acad. Sci. USA **111**, 12968 (2014).
[48] D. W. Moore, The Spontaneous Appearance of a Singularity in the Shape of an Evolving Vortex Sheet, Proc. Math. Phys. Eng. Sci. **365**, 105 (1979).
[49] R. H. Morf, S. A. Orszag, and U. Frisch, Spontaneous Singularity in Three-Dimensional Inviscid, Incompressible Flow, Phys. Rev. Lett. **44**, 572 (1980).
[50] R. B. Pelz and Y. Gulak, Evidence for a Real-Time Singularity in Hydrodynamics from Time Series Analysis, Phys. Rev. Lett. **79**, 4998 (1997).
[51] Y. Gulak and R. Pelz, High-symmetry Kida flow: Time series analysis and resummation, Fluid Dyn. Res. **36**, 211 (2005).
[52] A. J. Chorin, The evolution of a turbulent vortex, Commun. Math. Phys. **83**, 517 (1982).
[53] E. D. Siggia, Collapse and amplification of a vortex filament, Phys. Fluids **28**, 794 (1985).
[54] A. Pumir and E. Siggia, Collapsing solutions to the 3-D Euler equations, Phys. Fluids A **2**, 220 (1990).
[55] J. B. Bell and D. L. Marcus, Vorticity intensification and transition to turbulence in three-dimensional euler equations, Commun. Math. Phys. **147**, 371 (1992).
[56] R. B. Pelz, Locally self-similar, finite-time collapse in a high-symmetry vortex filament model, Phys. Rev. E **55**, 1617 (1997).
[57] R. Grauer and T. C. Sideris, Numerical Computation of 3D Incompressible Ideal Fluids with Swirl, Phys. Rev. Lett. **67**, 3511 (1991).
[58] R. Grauer, C. Marliani, and K. Germaschewski, Adaptive Mesh Refinement for Singular Solutions of the Incompressible Euler Equations, Phys. Rev. Lett. **80**, 4177 (1998).
[59] P. Orlandi and G. F. Carnevale, Nonlinear amplification of vorticity in inviscid interaction of orthogonal Lamb dipoles, Phys. Fluids **19**, 057106 (2007).
[60] S. S. V. Kolluru, P. Sharma, and R. Pandit, Insights from a pseudospectral study of a potentially singular solution of the three-dimensional axisymmetric incompressible Euler equation, Phys. Rev. E **105**, 065107 (2022).
[61] C. S. Campolina and A. A. Mailybaev, Chaotic Blowup in the 3D Incompressible Euler Equations on a Logarithmic Lattice, Phys. Rev. Lett. **121**, 064501 (2018).
[62] A. Larios, M. R. Petersen, E. S. Titi, and B. Wingate, A computational investigation of the finite-time blow-up of the 3D incompressible Euler equations based on the Voigt regularization, Theor. Comput. Fluid Dyn. **32**, 23 (2018).
[63] J. T. Beale, T. Kato, and A. Majda, Remarks on the breakdown of smooth solutions for the 3-D Euler equations, Commun. Math. Phys. **94**, 61 (1984).

[64] G. Ponce, Remarks on a paper by J. T. Beale, T. Kato, and A. Majda, Commun. Math. Phys. **98**, 349 (1985).
[65] P. Constantin, C. Fefferman, and A. J. Majda, Geometric constraints on potentially singular solutions for the 3-D Euler equations, Commun. Partial Differ. Equations **21** (1996).
[66] P. Constantin, Singular, weak and absent: Solutions of the Euler equations, Physica D **237**, 1926 (2008).
[67] G. L. Eyink, Dissipative anomalies in singular Euler flows, Physica D **237**, 1956 (2008).
[68] D. Chae, On the finite-time singularities of the 3D incompressible Euler equations, Commun. Pure Appl. Math. **60**, 597 (2007).
[69] J. Deng, T. Y. Hou, and X. Yu, Geometric Properties and Nonblowup of 3D Incompressible Euler Flow, Commun. Partial Differ. Equations **30**, 225 (2005).
[70] J. Deng, T. Y. Hou, and X. Yu, Improved Geometric Conditions for Non-Blowup of the 3D Incompressible Euler Equation, Commun. Partial Differ. Equations **31**, 293 (2006).
[71] T. Y. Hou and R. Li, Blowup or no blowup? The interplay between theory and numerics, Physica D **237**, 1937 (2008).
[72] C. Canuto, M. Y. Hussaini, A. Quarteroni, and T. A. Zang, Jr., *Spectral Methods in Fluid Dynamics* (Springer, Berlin, 2012).
[73] R. J. Leveque, *Numerical Methods for Conservation Laws* (Birkhäuser Verlag, Basel, Switzerland, 1990).
[74] S. S. Ray, U. Frisch, S. Nazarenko, and T. Matsumoto, Resonance phenomenon for the Galerkin-truncated Burgers and Euler equations, Phys. Rev. E **84**, 016301 (2011).
[75] D. Venkataraman and S. S. Ray, The onset of thermalization in finite-dimensional equations of hydrodynamics: insights from the Burgers equation, Proc. Math. Phys. Eng. Sci. **473**, 20160585 (2017).
[76] C. Sulem, P. L. Sulem, and H. Frisch, Tracing Complex Singularities with Spectral Methods, J. Comput. Phys. **50**, 138 (1983).
[77] M. D. Bustamante and M. Brachet, Interplay between the Beale-Kato-Majda theorem and the analyticity-strip method to investigate numerically the incompressible Euler singularity problem, Phys. Rev. E **86**, 066302 (2012).
[78] T. D. Drivas and H. Q. Nguyen, Remarks on the Emergence of Weak Euler Solutions in the Vanishing Viscosity Limit, J. Nonlinear Sci. **29**, 709 (2019).
[79] R. M. Pereira, R. Nguyen van yen, M. Farge, and K. Schneider, Wavelet methods to eliminate resonances in the Galerkin-truncated Burgers and Euler equations, Phys. Rev. E **87**, 033017 (2013).
[80] M. Farge, N. Okamoto, K. Schneider, and K. Yoshimatsu, Wavelet-based regularization of the Galerkin truncated three-dimensional incompressible Euler flows, Phys. Rev. E **96**, 063119 (2017).
[81] S. D. Murugan, U. Frisch, S. Nazarenko, N. Besse, and S. S. Ray, Suppressing thermalization and constructing weak solutions in truncated inviscid equations of hydrodynamics: Lessons from the Burgers equation, Phys. Rev. Res. **2**, 033202 (2020).
[82] R. M. Pereira, N. N. van yen, K. Schneider, and M. Farge, Adaptive solution of initial value problems by a dynamical Galerkin scheme, Multiscale Model. Simul. **20**, 1147 (2022).
[83] W. J. T. Bos and J.-P. Bertoglio, Dynamics of spectrally truncated inviscid turbulence, Phys. Fluids **18**, 071701 (2006).
[84] G. Krstulovic, P. D. Mininni, M. E. Brachet, and A. Pouquet, Cascades, thermalization, and eddy viscosity in helical Galerkin truncated Euler flows, Phys. Rev. E **79**, 056304 (2009).
[85] M. K. Verma, Boltzmann equation and hydrodynamic equations: their equilibrium and non-equilibrium behaviour, Philos. Trans. R. Soc. A. **378**, 20190470 (2020).
[86] M. K. Verma, S. Bhattacharya, and S. Chatterjee, Euler turbulence and thermodynamic equilibrium, arXiv:2004.09053.
[87] A. J. Majda and I. Timofeyev, Remarkable statistical behavior for truncated Burgers-Hopf dynamics, Proc. Natl. Acad. Sci. USA **97**, 12413 (2000).
[88] S. D. Murugan, Strain field from Galerkin-truncated Euler equation (2022), https://www.youtube.com/watch?v=4aql85cBYjE&ab_channel=SuganDuraiMurugan.
[89] P. Clark Di Leoni, P. D. Mininni, and M. E. Brachet, Dynamics of partially thermalized solutions of the Burgers equation, Phys. Rev. Fluids **3**, 014603 (2018).

[90] S. D. Murugan, Vorticity isosurfaces from Galerkin-truncated Euler equation (2022), https://www.youtube.com/watch?v=pEOUlGQnrsQ&ab_channel=SuganDuraiMurugan.
[91] A. J. Chorin, Turbulence and vortex stretching on a lattice, Commun. Pure Appl. Math. **39**, S47 (1986).
[92] S. D. Murugan, Perturbed vortex sheets showing onset of thermalization (2022), https://www.youtube.com/watch?v=yY8oelqtIzA&ab_channel=SuganDuraiMurugan.
[93] S. D. Murugan, Perturbed vortex sheets showing onset of thermalization (2022), https://www.youtube.com/watch?v=EgjBXp-WPOk&ab_channel=SuganDuraiMurugan.
[94] S. D. Murugan, Vortex sheets disturbed by Taylor-Green flow, showing onset of thermalization (2023), https://www.youtube.com/watch?v=tLebRP9swlw&ab_channel=SuganDuraiMurugan.
[95] S. D. Murugan, Perturbed vortex filament showing onset of thermalization (2023), https://www.youtube.com/watch?v=WTssHEXjn_4&ab_channel=SuganDuraiMurugan.
[96] P. E. Hamlington, J. Schumacher, and W. J. A. Dahm, Local and nonlocal strain rate fields and vorticity alignment in turbulent flows, Phys. Rev. E **77**, 026303 (2008).
[97] N. Fehn, M. Kronbichler, P. Munch, and W. A. Wall, Numerical evidence of anomalous energy dissipation in incompressible Euler flows: towards grid-converged results for the inviscid Taylor–Green problem, J. Fluid Mech. **932**, A40 (2022).